

# *Analysis of the main source regions of moisture transport events with the new ESA CCI/CM-SAF total column water vapour climate data record (v2)*

Article

Published Version

Creative Commons: Attribution-Noncommercial-No Derivative Works 4.0

Open Access

Eiras-Barca, J. ORCID: <https://orcid.org/0000-0003-4401-5944>, Algarra, I., Nieto, R., Schröder, M., Hegglin, M. I. ORCID: <https://orcid.org/0000-0003-2820-9044> and Gimeno, L. (2022) Analysis of the main source regions of moisture transport events with the new ESA CCI/CM-SAF total column water vapour climate data record (v2). Quarterly Journal of the Royal Meteorological Society, 148 (748). ISSN 1477-870X doi: <https://doi.org/10.1002/qj.4358> Available at <https://centaur.reading.ac.uk/107308/>

It is advisable to refer to the publisher's version if you intend to cite from the work. See [Guidance on citing](#).

To link to this article DOI: <http://dx.doi.org/10.1002/qj.4358>

Publisher: Royal Meteorological Society

All outputs in CentAUR are protected by Intellectual Property Rights law, including copyright law. Copyright and IPR is retained by the creators or other copyright holders. Terms and conditions for use of this material are defined in

the [End User Agreement](#).

[www.reading.ac.uk/centaur](http://www.reading.ac.uk/centaur)


## **CentAUR**

Central Archive at the University of Reading

Reading's research outputs online

## RESEARCH ARTICLE

# Analysis of the main source regions of moisture transport events with the new ESA CCI/CM-SAF total column water vapour climate data record (v2)

Jorge Eiras-Barca<sup>1,2</sup>  | Iago Algarra<sup>1</sup> | Raquel Nieto<sup>1</sup> | Marc Schröder<sup>3</sup> | Michaela I. Hegglin<sup>4,5</sup> | Luis Gimeno<sup>1</sup>

<sup>1</sup>Environmental Physics Laboratory (EPhysLab), CIM-UVIGO, Universidade de Vigo, Ourense, Spain

<sup>2</sup>Defense University Center at the Spanish Naval Academy, Marín, Spain

<sup>3</sup>Satellite-Based Climate Monitoring, Deutscher Wetterdienst, Offenbach, Germany

<sup>4</sup>Department of Meteorology, University of Reading, Reading, UK

<sup>5</sup>Institute of Energy and Climate Research—Stratosphere (IEK-7), Forschungszentrum Jülich, Jülich, Germany

## Correspondence

J. Eiras-Barca, Environmental Physics Laboratory (EPhysLab), CIM-UVIGO, Universidade de Vigo, Ourense, Spain.  
Email: [jeiras@uvigo.es](mailto:jeiras@uvigo.es)

## Funding information

Consellería de Cultura, Educación e Ordenación Universitaria, Xunta de Galicia, Grant/Award Number: ED431C 2017/64-GRC; European Space Agency, Grant/Award Number: 4000123554; Ministerio de Ciencia e Innovación, Grant/Award Number: RTI2018-0957772-B-I00

## Abstract

This study makes use of the new total column water vapour data record (CDR-2 (v2)), developed by the European Space Agency (ESA) in coordination with the Satellite Application Facility on Climate Monitoring (CM SAF), to analyse the adequacy of the integrated vertical water vapour column (IWV) data provided by the European Centre for Medium-Range Weather Forecasts (ECMWF) ERA5 and ERA-Interim reanalyses in regions of critical interest for moisture transport mechanisms. This information is critical for the initialization of moisture transport models—both Eulerian and Lagrangian—used to study the main mechanisms and predict the future evolution of moisture transport events. In particular, almost 40,000 atmospheric river (AR) and nocturnal low-level jet (NLLJ) events identified on a global scale between 2002 and 2017 have been used to study the variability between the cited reanalyses and CDR-2, in terms of both bias in the observed values of IWV during each particular event and daily temporal correlation fields. Although some notable discrepancies are reported in the main tropical rainforest regions, it is observed that, in regions of high interest for both ARs and NLLJs, the degree of agreement between the reanalyses and CDR-2 is high. The bias observed in the regions of interest is generally low, and the temporal correlation in the IWV fields is above 0.8 in most areas. ERA5 appears to show slightly better performance than ERA-Interim when resolving the moisture column, and both show greater similarity to CDR-2 in the midlatitudes compared with tropical regions. The probability density functions constructed on an event-to-event basis reinforce these ideas. We conclude that the evaluations presented here using CDR-2 serve to strengthen available evidence that the ECMWF reanalyses can safely be used in the initializations of Lagrangian dispersion models and Eulerian moisture tracer simulations—commonly used for the analysis of main advection mechanisms—in the vast majority of regions critical to the study of ARs and LLJs. They can also safely be used for the detection of moisture source–sink regions in the study of the global hydrological cycle in these regions.

## KEYWORDS

ERA5, ERA-Interim, moisture transport, total column water vapour

# 1 | INTRODUCTION

Atmospheric rivers (ARs) and nocturnal low-level jets (NLLJs) are acknowledged in the literature as the two main mechanisms of moisture transport in the troposphere (e.g., Gimeno *et al.*, 2016). Being responsible for most of the meridional transport of moisture and energy in the form of latent heat in the midlatitudes, both play a critical role in maintaining the radiative balance of the planet and the atmospheric branch of the hydrological cycle (e.g., Gimeno *et al.*, 2014; Algarra *et al.*, 2019b; Ralph *et al.*, 2020).

ARs are elongated regions—thousands of km long versus hundreds of km wide—of anomalous content of moisture in the lowest 2 or 3 km of the atmosphere, which are frequently associated with the pre-frontal regions of extratropical cyclones (e.g., Zhu and Newell, 1998; Gimeno *et al.*, 2014). Although there is a large consensus on the role played by ARs in the large-scale transport of moisture and latent heat by advection—often linked to the tropical moisture export (TME) mechanism (e.g., Knippertz and Wernli, 2010)—some studies have pointed out that a non-negligible part of the moisture associated with them is driven by local convergence mechanisms (e.g., Dacre *et al.*, 2015). The connection between the most intense ARs and extreme precipitation events—as well as the explosive deepening of pressure fields in cyclogenesis—has been demonstrated clearly in different parts of the world (e.g., Ralph and Dettinger, 2011; Lavers and Villarini, 2013; Dettinger *et al.*, 2015; Eiras-Barca *et al.*, 2016; 2018; Waliser and Guan, 2017). Despite this, some of the most recent results obtained by the community show the fundamental role played by the majority of ARs in the maintenance of the natural balance of the hydrological cycle, showing the “positive” role played by these. The most frequent events are of moderate intensity, and in some regions of the planet these moderate events are responsible for more than 40% of the total precipitation in the winter months (Ralph *et al.*, 2019; Eiras-Barca *et al.*, 2021). In particular, a positive role has also been demonstrated in that they may act as drought busters, for example on the U.S. West Coast (Dettinger, 2013). Additionally, there is a large consensus that the importance of ARs will increase for all the roles they play in the hydrological cycle in the near future, in the context of the atmosphere becoming hotter and wetter under a changing climate than under the current one (e.g., Lavers *et al.*, 2015; Ramos *et al.*, 2016b; Espinoza *et al.*, 2018; Massoud *et al.*, 2019). Figure 1a shows an example of a well-defined AR, observable in the field of integrated water vapour (IWV: Equation 1, where  $q$  is the specific humidity and  $\Omega$  denotes a vertical integration over the whole tropospheric column) reaching the Irish shore:

$$\text{IWV} = \frac{1}{g} \int_{\Omega} q \, dp. \quad (1)$$

For their part, NLLJs are frequently observed phenomena in different regions of the world. They can be detected as wind peaks located in the first 500 m of the troposphere in specific regions, tending to be semistationary seasonal events, particularly in summer months at night (Jiang *et al.*, 2007; Gimeno *et al.*, 2016; Algarra *et al.*, 2019b, and references therein). The formation mechanism is not fully understood yet. In any case, a combination of the Blackadar (1957) mechanism and the Holton (1967) mechanism is considered to explain most of the events (e.g., Algarra *et al.*, 2019b). On the one hand, the Blackadar mechanism proposes that NLLJs are the result of inertial oscillations of the ageostrophic wind, triggered by a sudden decay of turbulence in the boundary layer after sunset. On the other hand, the Holton mechanism emphasizes the role played by thermal forcing in the diurnal oscillation of the boundary-layer wind, as a consequence of sloping terrain. Figure 1b shows an example of the well-known Great Plains Low-Level Jet, which is responsible for a great intrusion of moisture into the North American continent, the main sources of which being the Gulf of Mexico and the Caribbean Sea.

Simulations of moisture transport processes are indispensable tools for a detailed understanding of these phenomena. The correct identification of source and sink regions, as well as advective processes that distribute moisture between the different regions of the planet, is essential to properly understand and predict the evolution of the hydrological cycle and the incidence of extreme hydrological events such as droughts or floods on a global scale (e.g., Gimeno *et al.*, 2020).

Although there are numerous tools for the simulation of moisture transport processes, all of them fall more or less exactly into two well-defined formalisms: Lagrangian dispersion models and Eulerian models. In relation to the former, we highlight the role played by the Flexpart dispersion model (Stohl *et al.*, 2005), with which numerous studies have been carried out that have made it possible to identify the source and sink regions of the main transport phenomena accurately (e.g., Nieto *et al.*, 2010; Gimeno *et al.*, 2013; 2020; Ramos *et al.*, 2016a). Regarding the latter, moisture tracer tools coupled to mesoscale Eulerian models provide accurate information on transport phenomena, allowing a detailed study of not only the origin and fate of the moisture itself, but also all the physics involved in the processes. In this sense, the Weather Research and Forecasting (WRF) water vapour tracers tool (WRF-VT: Insua-Costa and Miguez-Macho, 2018), which has been used for some years to understand the processes associated with both ARs and NLLJs—as well as other relevant



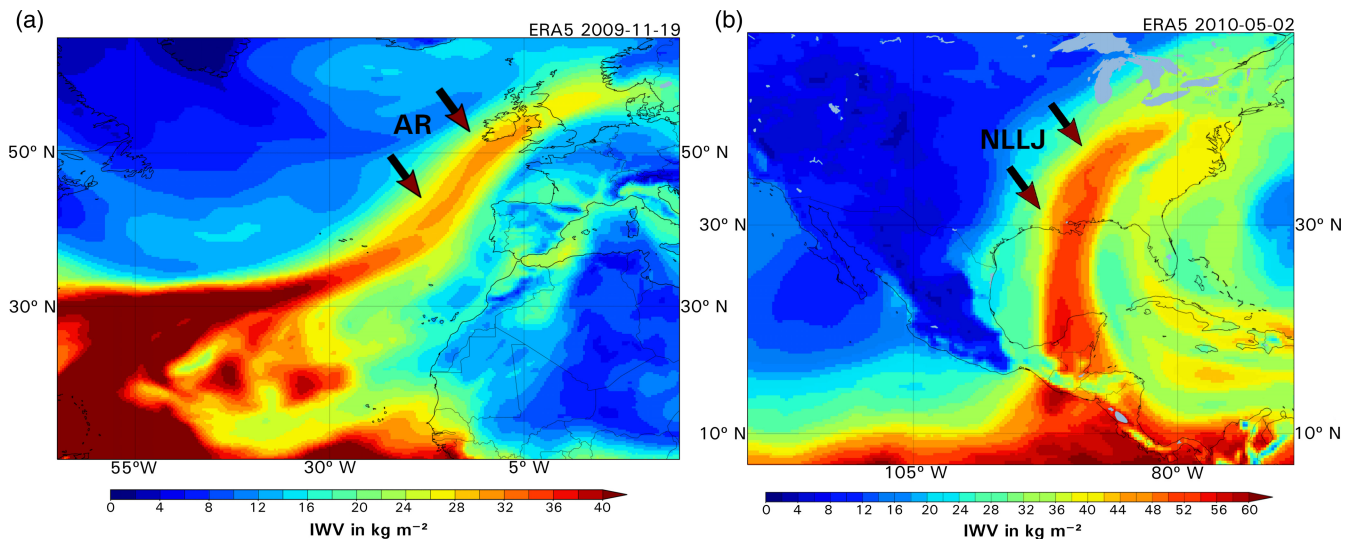


**FIGURE 1** (a) Example of an AR reaching the coast of Ireland, in the fields of IWV on November 11, 2009. (b) Example of a Great Plains Low-Level Jet bringing an intrusion of air rich in Atlantic moisture into the North American continent on May 2, 2010. IWV has been retrieved from the ERA5 reanalysis (Hersbach *et al.*, 2020) at  $0.25^\circ \times 0.25^\circ$  horizontal resolution. The arrows show the main axis of both AR and NLLJ events in a and b respectively. [Colour figure can be viewed at [wileyonlinelibrary.com](http://wileyonlinelibrary.com)]

mechanisms such as the monsoon circulations—better, is worth mentioning (Dominguez *et al.*, 2016; Eiras-Barca *et al.*, 2017; Algarra *et al.*, 2019a).

All models designed to analyse moisture transport phenomena, without exception, rely on reanalysis models to feed their initial and boundary conditions. Because of the nature of moisture transport, the information on moisture content in the vertical column that these reanalysis models provide to the transport models is essential information that must be accurate for the results and conclusions obtained to be objective and realistic. Moisture content in the atmosphere is a complex variable, which depends on the interaction between all the components of the climate system. Detailed studies on moisture transport usually rely on coupled models that go beyond simple moisture transport, and take into account complex land–atmosphere interactions (e.g., Eiras-Barca *et al.*, 2020). However, the Eulerian and Lagrangian models mentioned above rely solely on the information on moisture content provided by the reanalysis models, which are of a global and holistic nature and do not take into account, for example, the essential role played by groundwater (Miguez-Macho and Fan, 2012).

Accurate observational data of moisture content in the atmosphere—for example, high-resolution satellite products such as the one used in this work—can help determine whether the information provided by the global reanalyses and fed into moisture transport simulation models can be deemed realistic and reliable. In this article, we make use of the Climate Change Initiative (CCI)/CM SAF total water column climate data record

merged within the recent European Space Agency (ESA) Water Vapour Climate Change Initiative, to provide—in a so-called validation exercise—a thorough comparison between these satellite observations and the information obtained from the two most widely used reanalyses, ERA5 and ERA-Interim. More than 39,000 ARs and NLLJ events stored in our database have been analysed. The main objective is to determine the degree of reliability of the moisture content information provided by these reanalyses, and thus of the results provided by the transport models that use them as initial and boundary conditions for their simulations. The cited transport models are used to determine not only moisture source and sink regions, but also predictable changes in transport phenomena in the near future.

Finally, it is noteworthy to comment that, as part of the project, the climate data record version 2 (CDR-2) is already being used in different areas from a user application perspective. For example, He *et al.* (2022) used CDR-2 to evaluate the interannual variability of ERA5 and the global climate models included in the Coupled Model Intercomparison Project Phase 6 (CMIP6), with focus on the tropical belt. The German Aerospace Center (DLR) is also working with this data jointly with cloud data for CMIP evaluations. The precursor version of CDR2 from ESA, DUE GlobVapour Special sensor microwave/imager+Medium Resolution Imaging Spectrometer (SSM/I+MERIS), was used in intercomparison studies by Schröder *et al.* (2018) and can also be used to intercompare results from trend analysis, similarly to Schröder *et al.* (2019). A key advantage of CDR-2 is its high

resolution over land, where it can be particularly useful to support process studies (e.g., Carbajal Henken *et al.*, 2015) and process improvement in model development studies. It may also be useful for data assimilation, as discussed in Saunders (2021).

## 2 | METHODS

### 2.1 | CCI/CM SAF water vapour climate data record (v2)

The global total column water vapour (TCWV) data record combines microwave and near-infrared (NIR) imager-based TCWV over the ice-free ocean as well as over land, coastal ocean, large inland water bodies, and sea ice, respectively. The data record relies on microwave observations from the Special Sensor Microwave Imager (SSM/I), Special Sensor Microwave Imager/Sounder (SSMIS), Advanced Microwave Scanning Radiometer (AMSR-E), and Tropical Rainfall Measuring Mission (TRMM) Microwave Imager (TMI). This dataset is based partly on a fundamental climate data record (Fennig *et al.*, 2020) and on near-infrared observations from the Medium Resolution Imaging Spectrometer (MERIS, 3rd reprocessing), Moderate-Resolution Imaging Spectroradiometer (MODIS-Terra, collection 6.1), and Ocean and Land Colour Instrument (OLCI, 1st reprocessing). The NIR-based retrieval relies on differential absorption using observations at 890–900 nm, while key information in the microwave observations is contained at around 23 GHz. In both cases, a one-dimensional variational analysis is utilised to retrieve TCWV. Reliable retrievals are not possible in the presence of heavy precipitation (microwave observations), in the presence of clouds, and during the night (NIR observations). Due to low reflectivities, the TCWV quality is reduced over coastal waters. Further details of the retrieval are described in Andersson *et al.* (2010) and Graw *et al.* (2017) for the microwave imagers, as well as in Lindstrot *et al.* (2012), Diedrich *et al.* (2015), and Fischer *et al.* (2021) for the near-infrared imagers. The water vapour of the atmosphere is vertically integrated over the full column and given in units of  $\text{kg}\cdot\text{m}^{-2}$ . Both the microwave—defined over the open ocean—and NIR—defined over land and used to fill spatial gaps such as those shown on coasts, sea-ice, and large inland bodies—data streams are processed fully independently. After the processing of gridded microwave and NIR-based TCWV data, the spatial complementarity is used to combine both data sets into a global data set. During this process, microwave and NIR-based data sets are not averaged or interpolated by any means and thus the individual TCWV values and their uncertainties remain valid.

**TABLE 1** Periods into which the study is divided, corresponding to the five different data sources considered in CDR-2

ID	Period	Data source
P1	2002-07 to 2010-12	meris-cmsaf, hoaps
P2	2011-01 to 2012-03	meris-modis, terra-cmsaf, hoaps
P3	2012-04 to 2016-03	modis, terra-cmsaf, hoaps
P4	2016-04 to 2016-12	olci-modis, terra-cmsaf, hoaps
P5	2017-01 to 2017-12	olci-cmsaf, hoaps

The combined data record has a spatial resolution of  $0.5^\circ \times 0.5^\circ$  or  $0.05^\circ \times 0.05^\circ$ , with the NIR-based data being averaged and the microwave-based data being oversampled to match the lower (respectively higher) spatial resolution. The product is available as daily and monthly means and covers the period July 2002–December 2017. Here, version 2 from ESA CCI was used, while the official release of the final version 3 is planned in 2022 by CMSAF.<sup>1</sup>

For the purpose of this study, we divided the data into five different periods, according to the sensors and constellations used for the generation of CDR-2. Table 1 shows this division, along with the corresponding spectrometers and constellations implicated.

### 2.2 | AR and NLLJ database

In order to perform a more detailed analysis of the relationship between the reanalyses used and CDR-2, the moisture source regions of interest associated with ARs were divided into three regions (midlatitudes Northern hemisphere, midlatitudes Southern hemisphere, and tropical regions). Similarly, the NLLJs have been divided into four regions, according to the origin of the major moisture income (midlatitude land, midlatitude ocean, tropical land, tropical ocean), as detailed in Table 2.

The detection of NLLJ events is applied following the methodology described in Algarra *et al.* (2019b), which in turn is based on the methodology of Rife *et al.* (2010). The identification of NLLJs is thereby based on the temporal variation of the vertical structure of the wind and on the fact that the NLLJs are most intense at local midnight. Thus, a climatology is developed for the summer months in both hemispheres (July for boreal summer and January for austral summer), where a NLLJ event is identified if (i) the wind speed is higher at local midnight than at midday, and (ii) the local midnight wind speed is higher at the surface (500 m) than above (4 km). For

<sup>1</sup>For questions, contact [contact.cmsaf@dwd.de](mailto:contact.cmsaf@dwd.de)

**TABLE 2** Division applied to the AR (top) and NLLJ (bottom) events in the study

AR source	AR source ID
Midlatitude NH (lat. $\geq 30$ )	R18, R12, R01, R09, R13, R07, R10, R03, R02, R08, R11
(Sub)tropics	R06, R20, R19, R17
Midlatitude SH (lat. $\leq -30$ )	R21, R05, R14, R23, R22
LLJ source	LLJ source ID
Midlatitude (lat. $\geq \pm 25$ ) Land	4, 8, 26, 27, 28, 29
Midlatitude (lat. $\geq \pm 25$ ) Ocean	2, 3, 9, 10, 14, 18, 19, 20, 21, 22, 23, 24, 25, 30
Tropics land	5, 6, 7, 11, 12, 13, 15, 16, 17
Tropics ocean	1, 31, 32, 33

Note: AR and NLLJ source IDs will be used in subsequent figures.

identification of the subsequent sources of moisture, the Lagrangian model FLEXible PARTicle (FLEXPART; Stohl and James, 2004; Stohl *et al.*, 2005) is used once the regions of maximum occurrence of NLLJs have been detected. FLEXPART is used to identify the sources of moisture linked with each one of the NLLJs identified globally. Detailed information on this methodology can be found in Algarra *et al.* (2019b).

As for the ARs, the areas of maximum occurrence of land-falling ARs (LARs), were identified following the methodology of Algarra *et al.* (2020). Therefore, areas with a higher frequency than 10% of the total number of LAR days for the study period (2002–2017) and associated with a negative mean sea-level pressure anomaly are detected as regions of maximum occurrence of LAR. Then, the Lagrangian model FLEXPART is used to detect anomalous moisture uptake (AMU) areas associated with each previously detected LAR event. Thus, AMU was obtained from the difference between the moisture uptake of each individual LAR event and the climatological moisture uptake for the LAR day over the period 2002–2017. More information on this methodology can be found in Algarra *et al.* (2020).

Finally, centroids were calculated based on weighted moisture distributions within the moisture source regions during events presenting the two major mechanisms of atmospheric moisture transport analysed in this study, NLLJs and ARs. For example, if the highest evaporation values within the region labelled as a source of moisture are concentrated in a certain area, the centroid will be displaced towards that region. These centroids are the points used at each event in the intercomparison between CDR-2 and both reanalyses to build the probability density functions shown in Section 3.4, as detailed below. Regions on which we will focus the study—for both ARs and LLJs—are shown in Figure 2.

## 2.3 | Intercomparison methodology

The goal of this research is the intercomparison of IWV values using three different data sources: on the one hand, the reanalyses from the European Centre for Medium-Range Weather Forecasts (ECMWF) 5th Re-Analysis (ERA5: Hersbach *et al.* (2020),  $0.25^\circ \times 0.25^\circ$ , 6 hr) and Interim Re-Analysis (ERAIn: Dee *et al.* (2011),  $0.75^\circ \times 0.75^\circ$ , 6 hr), and on the other hand the low-resolution version of CDR-2 ( $0.5^\circ \times 0.5^\circ$ , 24 hr), which is described in more detail above. A bilinear interpolation (extrapolation) has been applied to the reanalysis data in order to upscale (downscale) the grids into a unified grid of  $0.5^\circ \times 0.5^\circ$ , coincident with the original resolution of CDR-2.

For the periods P1–P5 (see Table 1), the mean bias has been calculated between both ERA5 and ERAIn versus CDR-2 across the whole domain. Regions of relevance for AR and NLLJ moisture uptake are highlighted in the resulting maps, in order to allow easy identification and comparison with other regions in the world.

The same distribution into five periods has been applied to calculate the daily temporal correlations between both ERA5 and ERAIn versus CDR-2 data. The Spearman temporal correlation coefficient, as a non-parametric alternative to Pearson's temporal correlation (Myers and Sirois, 2004), has been calculated at each point of the domain for each period of interest. This procedure has been applied in order to identify regions in the world where the correlation between the reanalyses and the comprehensive observations is at a maximum or minimum and to determine whether they coincide with regions of interest for moisture transport processes.

Finally, using more than 31000 AR events and 8300 NLLJ events stored in our database, we created a series of probability density functions (PDFs) of the bias between

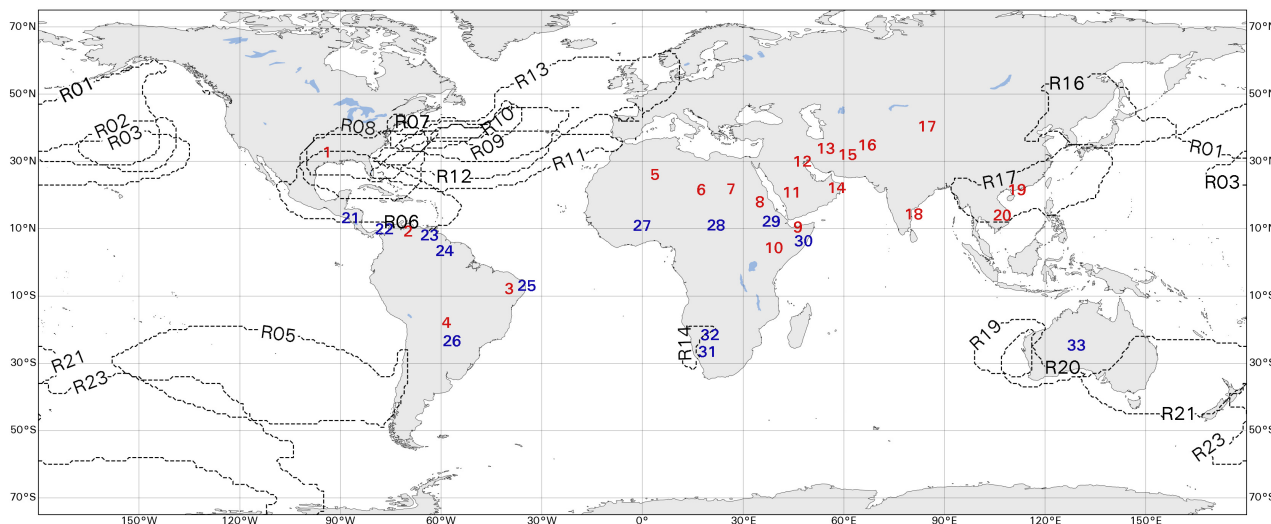


**FIGURE 2** Regions of interest for main moisture transport mechanisms. Regions of anomalous moisture uptake for AR activity are labelled with “R” within the contours. The main planetary NLLJs are also shown with numbers between 1–20 and 21–33 for July and January NLLJs, respectively [Colour figure can be viewed at [wileyonlinelibrary.com](http://wileyonlinelibrary.com)]

each reanalysis and CDR-2. In this case, we considered not only the five natural periods, but also a division based on latitudinal criteria, depending on the location of their main moisture sources, as detailed in Table 2. In the case of NLLJs, there is no event in our database corresponding to P5, so only P1–P4 have been considered in the analysis. Additionally, only the months of January or July have been considered in the NLLJ analysis, as they are the most active months, depending on the hemisphere. For each event, the bias has been calculated at the point of the centroid of the AR or NLLJ path, as described in detail in the previous section.

### 3 | RESULTS AND DISCUSSION

#### 3.1 | Bias fields

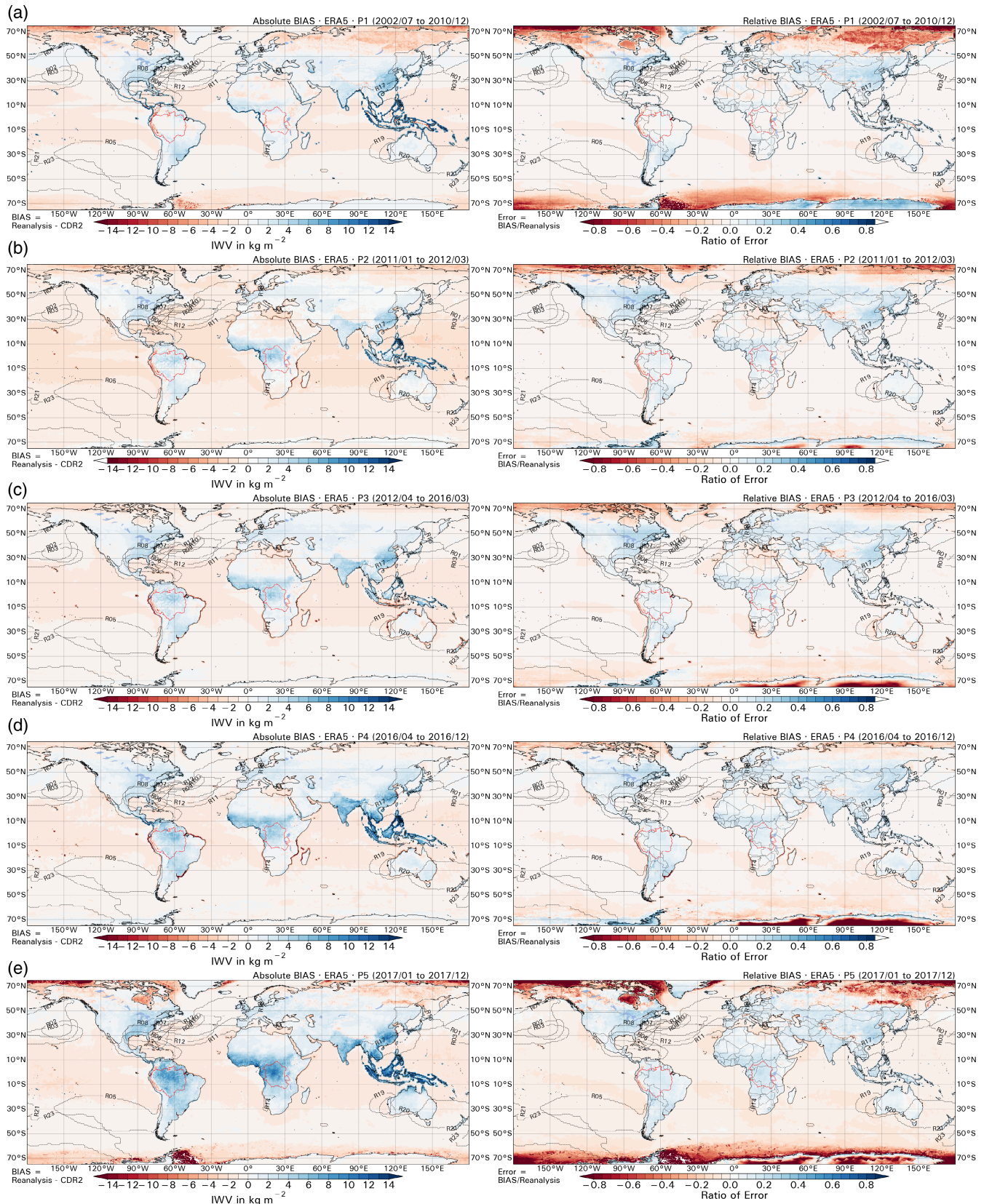
Figure 3 shows the average bias (Reanalysis – CDR-2) between ERA5 and CDR-2, built from monthly mean fields of the reanalysis and the observational data for each corresponding period. The left column represents the total bias of IWV in  $\text{kg}\cdot\text{m}^{-2}$  (or mm) and the right column represents the relative bias (bias/reanalysis) as a percentage. Each row corresponds to a period, starting with P1 and ending with P5. Regions of interest for anomalous moisture uptake in AR events are indicated with black contours and labelled with the letter “R”. Regions of high NLLJ activity are labelled with blue or red numbers, depending on whether their peak activity is in January or July, respectively.

As can be seen, the regions of importance for both transport phenomena are generally located in areas with

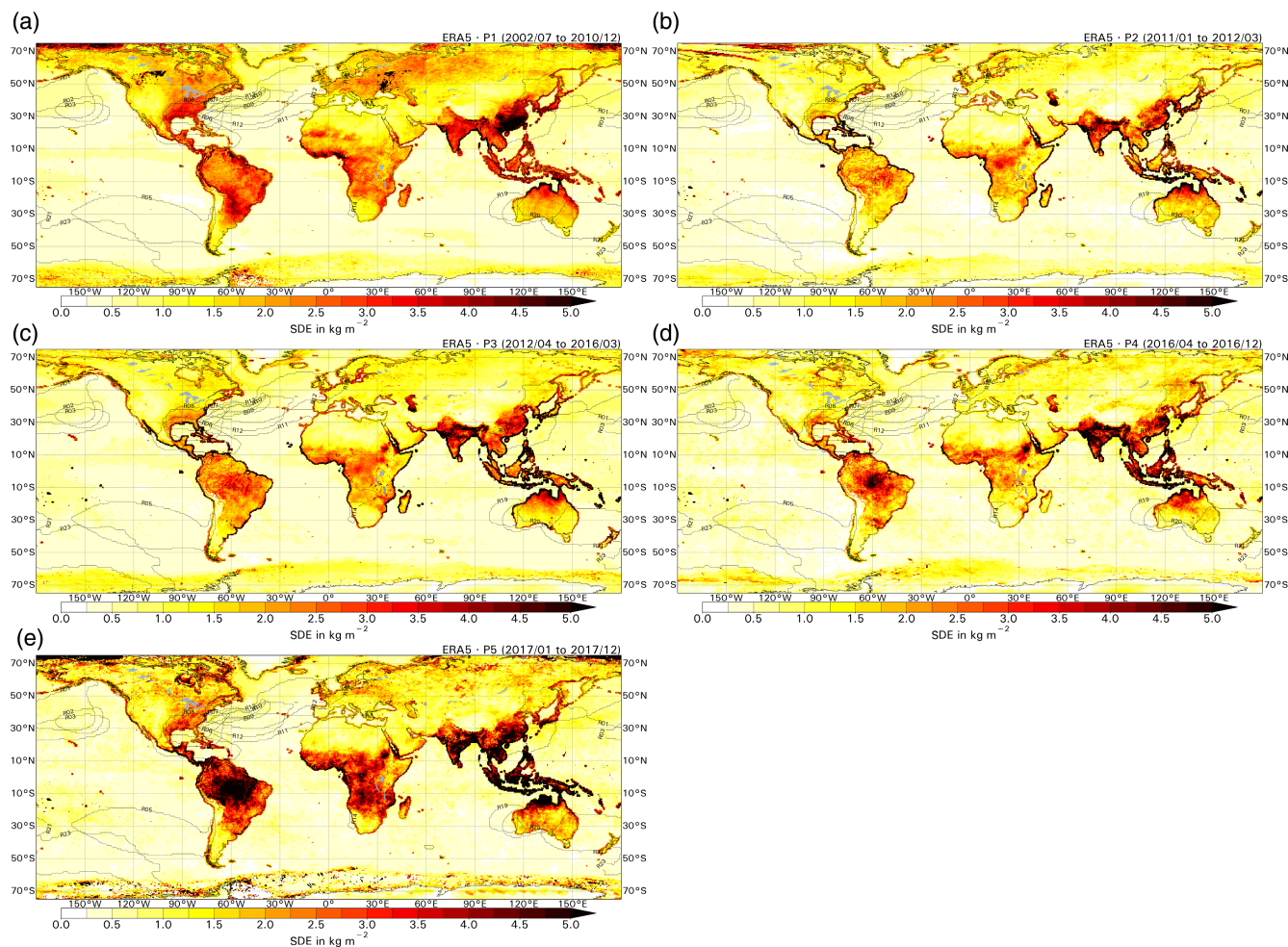
very moderate bias (mostly between  $-2$  and  $0 \text{ kg}\cdot\text{m}^{-2}$ ). Although NLLJs are located over land, their moisture source regions are also oceanic, and all biases are moderate over the ocean when we compare ERA5 with CDR-2. On the other hand, these biases tend to increase in tropical regions, so it can be concluded that ERA5 resolves the IWV column better in midlatitudes. Particularly noteworthy is the positive bias observed in the three large tropical forests in P5 (January–December 2017, olci-cmsaf hoaps), with some values exceeding  $6 \text{ kg}\cdot\text{m}^{-2}$  on average. This might also be caused by differences in sampling (see below). However, these tropical forests are not a source of moisture for any active ARs and, although they are located close to some NLLJ activity zones, they are not considered source regions for any of them either. Therefore, there is no reason to believe that the discrepancies between ERA5 and CDR-2 in these regions would affect the transport simulations in any way. Results compatible with these have been observed by Yu *et al.* (2021), who analysed differences in IWV between ERA5 and observations from the stations of the Global Positioning System between 2016 and 2018. Even though they lack data from the tropical rainforest or over the ocean, they detected, for example, a consistent positive bias of up to  $2 \text{ kg}\cdot\text{m}^{-2}$  over North America or Europe.

Figure S1 in the Supplementary Material shows identical information to that for Figure 3, but comparing ERAIn versus CDR-2 instead of ERA5 versus CDR-2. As can be seen, there are no notable differences with respect to the conclusions obtained with ERA5. Again, reduced bias is observed in the oceanic regions of interest for these transport phenomena, and a higher bias is seen over tropical regions. The assignment of each





**FIGURE 3** The left column shows the mean absolute bias between ERA5 and CDR-2 (bias = ERA5–CDR-2) in  $\text{kg m}^{-2}$  (or mm). These values have been calculated based on the monthly means of both the reanalysis and CDR-2 for the five periods of interest (P1–P5, top to bottom rows). The right columns show the relative bias (bias/ERA5) of the corresponding subfigures on the left. Regions of interest for AR activity are labelled with “R” within the contours. The main planetary NLLJs are also shown with numbers between 1–20 and 21–33 for July and January NLLJs, respectively [Colour figure can be viewed at [wileyonlinelibrary.com](http://wileyonlinelibrary.com)]



**FIGURE 4** Standard deviation of the errors between CDR-2 and ERA5 in  $\text{kg}\cdot\text{m}^{-2}$  for each period of interest. Regions of anomalous moisture uptake for AR activity are labelled with black contours for easier interpretation [Colour figure can be viewed at [wileyonlinelibrary.com](http://wileyonlinelibrary.com)]

of the regions of interest for transport phenomena (as seen in Figure 3) to each of these zones can be seen in Table 2.

### 3.2 | Standard deviation of the errors

Figure 4 shows the standard deviation of errors (SDE) calculated on a monthly basis for each of the study periods assessing the degree of coincidence between CDR-2 and ERA5. Overall, it is observed that the highest SDEs—identifying regions where the differences between the IWV values reported by CDR-2 and ERA5 are higher—are restricted to terrestrial (sub)tropical latitudes. In particular, high dispersion is observed in the watersheds of large tropical forests, as well as in major monsoon regions.

The period with the largest discrepancy is P5, corresponding to the olci-cmsaf hoaps sensors combination. In

this period, most of the tropical regions show SDEs higher than  $5 \text{ kg}\cdot\text{m}^{-2}$ .

Regarding the main mechanisms of moisture transport, it is observed that the vast majority of the regions of interest for the AR phenomenon are located in areas with low SDEs. As an exception to this observation, regions R06, R07, and R08 (corresponding to the Gulf of Mexico coast) and regions R19 and R20 (corresponding to the Australian west coast) show values close to  $3 \text{ kg}\cdot\text{m}^{-2}$ , which can be considered relatively high. This must be taken into account when analysing the reliability of the results related to the identification of source and sink regions in these areas in past and future studies.

Figure S2 in the Supplementary Material shows fields analogous to those discussed in the previous paragraph, however for the comparison between CDR-2 and ERA-Interim. As can be observed, no remarkable differences are shown, since the ESD fields are practically identical to those presented in Figure 4. The conclusion, therefore, that



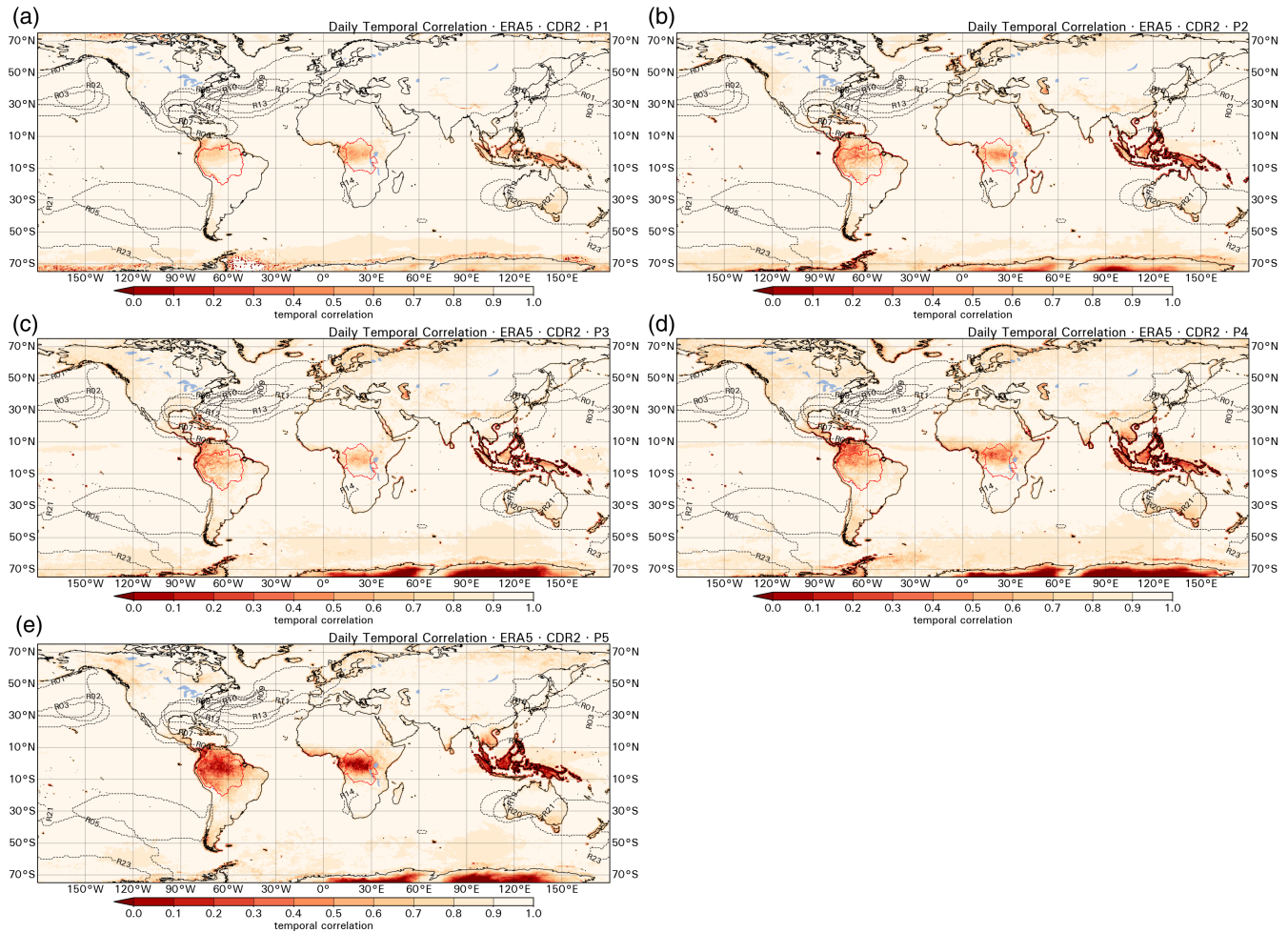


**FIGURE 5** Temporal correlation between daily ERA5 and CDR-2 data. The five rows correspond to the five periods of interest (a–e correspond to P1–P5). Regions of interest for AR activity are labelled with “R” within the contours. The main planetary NLLJs are also shown with numbers between 1–20 and 21–33 for July and January NLLJs, respectively [Colour figure can be viewed at [wileyonlinelibrary.com](http://wileyonlinelibrary.com)]

simulations intended to evaluate sources and sinks should be treated with care in regions where the SDE is high is also valid for the case of simulations initialized with ERA-In.

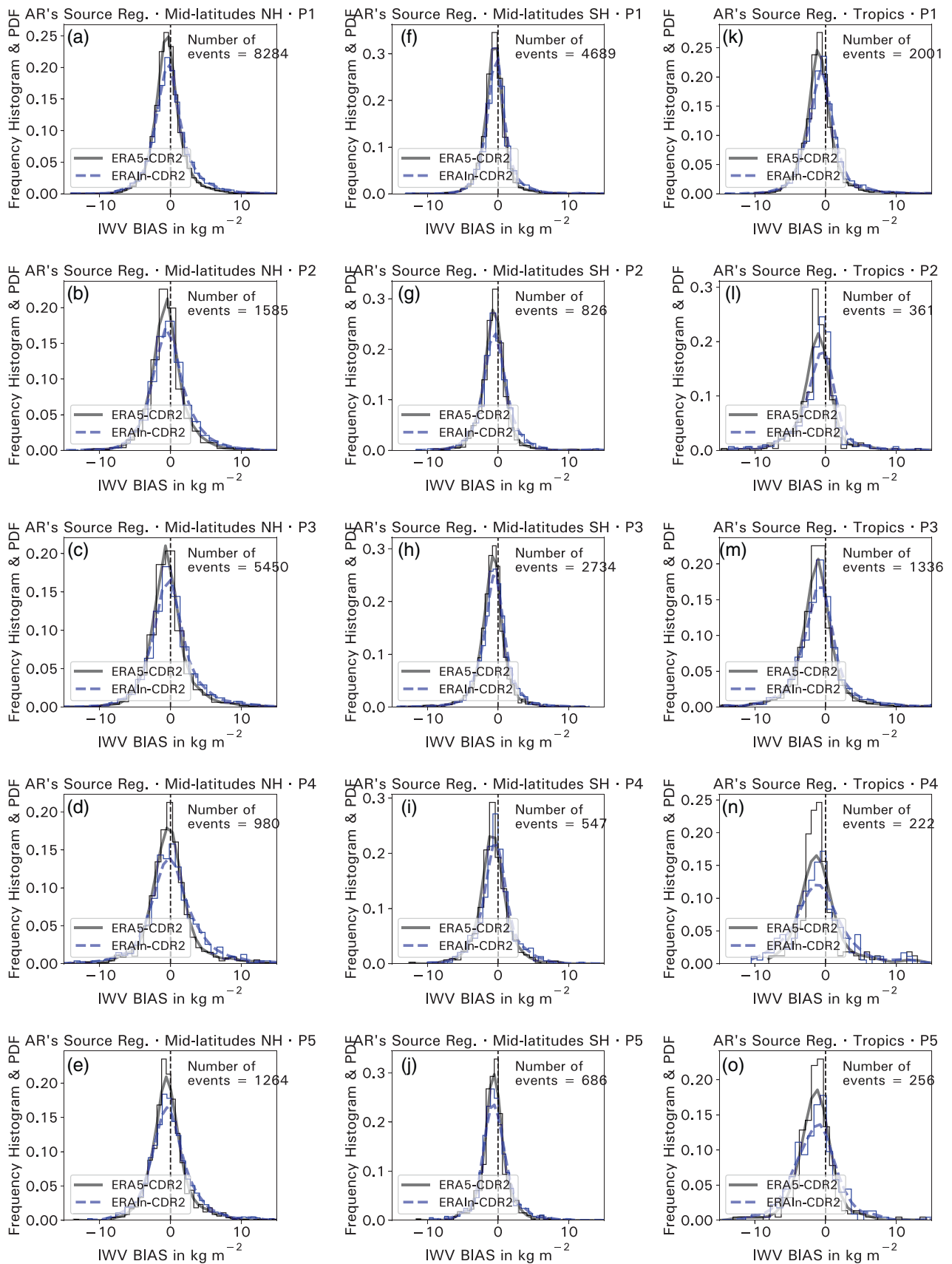
### 3.3 | Daily temporal correlations

Figure 5 shows daily temporal correlations calculated between ERA5 and CDR-2 for P1–P5. As can be seen, most of the regions of interest—in the mid-latitudes—present correlation values higher than 0.8, which implies good temporal correlations. Again, it is the tropical regions, particularly tropical forests, that show the largest discrepancies between ERA5 and CDR-2, as discussed further below. Particularly noteworthy in this regard is the case of P5, where correlation values drop to 0.2. In spite of this, as we have indicated above, these tropical forests are not the main source of moisture for ARs and NLLJs, thus in

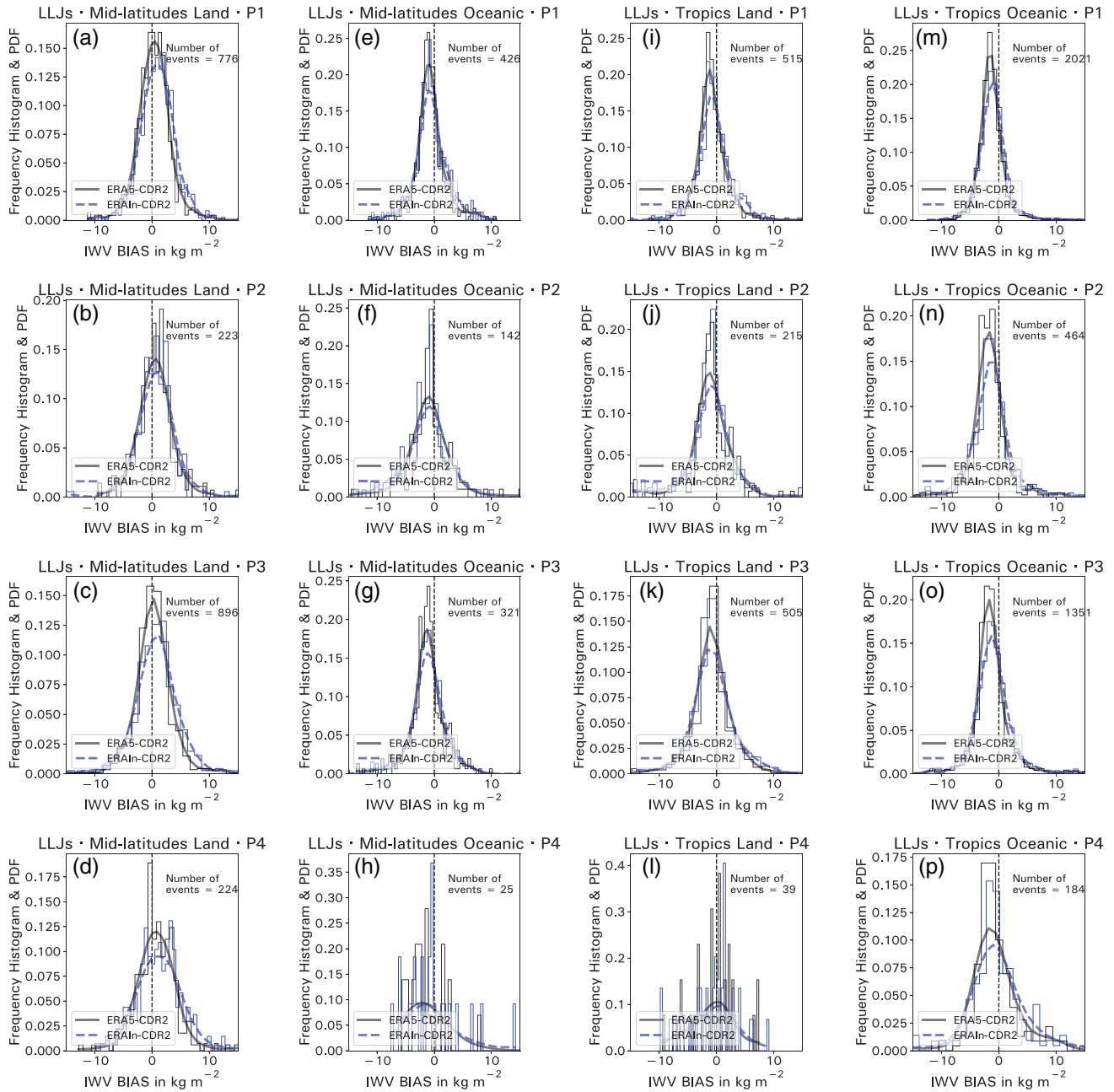
the main regions of interest the daily temporal correlation results remain high.

Figure S3 in the Supplementary Material shows the same temporal correlations calculated for ERAIn versus CDR-2. As can be seen, although the results are similar, the temporal correlations are better for ERA5 when compared with ERAIn. The above statement is particularly true for the oceanic regions and the P3 period. Particularly notable is the fact that in all distributions—for both ARs and LLJs—the dispersions presented by ERA5 are substantially lower than those presented by ERAIn. This fact again reinforces the idea that the degree of agreement between CDR-2 and ERA5 is notably higher than the degree of agreement between CDR-2 and ERAIn.

It is important to take into account at this point the temporal divergence that exists between the two data sources. The reanalysis data have been obtained every 6 hr, having performed the daily average of four time steps to



**FIGURE 6** Probability density functions (PDF) of bias between both ERA5 versus CDR-2 (solid lines) and ERAIn versus CDR-2 (dashed lines) for AR events detected from 2002–2017. Columns present the PDFs following the regional distribution shown in Table 2. Rows present the PDFs following the temporal distribution shown in Table 1 [Colour figure can be viewed at [wileyonlinelibrary.com](http://wileyonlinelibrary.com)]



**FIGURE 7** Probability density functions (PDF) of bias between both ERA5 versus CDR-2 (solid lines) and ERAIn versus CDR-2 (dashed lines) for NLLJ events detected from 2002–2016. Columns present the PDFs following the regional distribution shown in Table 2. Rows present the PDFs following the temporal distribution shown in Table 1. P5 is missing in this plot, since the NLLJ database used in this analysis covers only P1–P4 [Colour figure can be viewed at [wileyonlinelibrary.com](http://wileyonlinelibrary.com)]

obtain the value of that day. For their part, the underlying temporal resolution of the daily mean values of the CDR depends on the sensor–constellation combination. The observations over land rely on MERIS, MODIS, and OLCI data. Each satellite has an Equator-crossing time of approximately 10:30 local time, in sun-synchronous orbit. Thus, the daily average over land consists of a sample at ~10:30 local time. Over ocean, significantly more satellites are used and, in particular, also data obtained from low Earth orbits. The latter have a fairly decent

coverage of the diurnal cycle, at least over the Tropics and up to ~45°–55°, depending on the satellite. Thus, over ocean the product may be considered as a daily average.

### 3.4 | Probability density functions of bias

Figure 6 shows the probability density functions of the bias between CDR-2 and both ERAIn (blue line) and

ERA5 (black line). Along with the five periods (P1–P5), the domain has been divided into three regions, according to Table 2. In general, slightly negative differences are observed in the bias—particularly for ERA5—which means that the reanalysis models tend to underestimate IWV values (with differences close to  $2 \text{ kg} \cdot \text{m}^{-2}$  on average) in strategic regions for AR activity. These results are consistent with those shown in Figure 3, where dry biases were observed over ocean regions that are also critical regions for AR activity. Again, the largest differences are observed over the Tropics, particularly in periods P4 and P5. Despite this, most distributions show a clear leptokurtik kurtosis, revealing a good degree of coincidence. Once again, it is essential to take into account that each event has a temporal resolution of 6 hr in the reanalysis. There may be potential differences of up to 18 hr between the satellite measurement and the time at which the AR event occurred, adding some variability to the derived bias.

As for the NLLJs, Figure 7 shows the probability density functions of the bias between CDR-2 and both ERAIn (blue line) and ERA5 (black line). In this case, and due to the nature of these phenomena, we propose a division into four regions, depending on the location not of wind maxima but of moisture sources. In general, as in the case of ARs, a slight shift to the left of the distributions is observed, indicating that the reanalyses tend to underestimate the moisture content observed by CDR-2. As indicated, in this case we do not have events in P5 in the NLLJ database, so we restrict the analysis to periods P1–P4. Again, it is observed that the bias tends to be slightly higher in tropical regions compared with the midlatitudes. In any case, almost all distributions again show leptokurtik kurtosis. Note that, in the case of Figure 7h,i, the number of events is insufficient (25 and 39, respectively), so the distribution lacks statistical significance.

In relation to the differences observed between ERA5 and ERAIn in their comparison with CDR-2, a greater spread is observed for the ERAIn curves in all cases, which denotes a greater agreement with ERA5. This result is to be expected from the latest generation of reanalysis models.

## 4 | CONCLUSION

The new satellite climate data record, CCI/CM SAF total column water vapour over land and ocean (or CDR-2) as obtained from the Water Vapour CCI, is utilised in this study. In particular, this CDR has been used to test the degree of agreement with the most frequently used reanalyses in Eulerian and Lagrangian moisture transport models used to study source regions of moisture transport events: ERA5 and ERAIn.

Although some discrepancies are reported in tropical regions—that is, in tropical forests—the agreement between CDR-2 and the reanalyses is high in the regions of interest for moisture input into ARs and NLLJs. The agreement has been tested with bias maps for the five periods of interest into which CDR-2 is divided, with daily correlation fields, and bias probability density functions using more than 31,000 AR events and 8300 NLLJ events that were detected objectively.

In general, the regions of interest for these phenomena show a small mean bias in IWV—mostly less than  $\pm 2 \text{ kg} \cdot \text{m}^{-2}$ —and daily correlations greater than 0.8. As for the distributions of the more than 39,000 events, they are mainly centred on values between  $-3$  and  $0 \text{ kg} \cdot \text{m}^{-2}$ . For both NLLJs and ARs, it is observed that tropical regions tend to show a slightly higher bias, and that ERAIn exhibits a higher dispersion than ERA5, highlighting a better agreement between CDR-2 and ERA5.

It is concluded that CDR-2 provides a useful tool for providing evidence that ERA5 and ERAIn reanalyses can safely be used for the initiation of Eulerian and Lagrangian simulations of moisture transport phenomena in the vast majority of those regions critical for the study of ARs and LLJs, mainly centred on (sub)tropical and mid—usually oceanic—latitudes. For polar and tropical—mainly continental—regions, these results show a larger discrepancy between reanalyses and CDR-2. This suggests that conclusions regarding the hydrological cycle and the analysis of transport phenomena obtained with simulations over these regions should be treated with greater caution. These discrepancies occur mainly in tropical forest regions, which are not areas of critical interest for moisture transport phenomena and are therefore beyond the scope of this article. They are currently the subject of further study. A possible explanation is that reanalyses do not assimilate NIR observations (SPARC, 2022, table 2.21) or that these only allow reliable retrievals under clear-sky conditions, which are infrequent in tropical rainforests.

The potential of the new CDR-2 IWV database for multiple other potential user applications is also revealed.

## AUTHOR CONTRIBUTIONS

**Jorge Eiras-Barca:** conceptualization; data curation; formal analysis; investigation; methodology; software; validation; visualization; writing – original draft; writing – review and editing. **Iago Algarra:** formal analysis; investigation; methodology; visualization. **Raquel Nieto:** funding acquisition; project administration; supervision; writing – original draft; writing – review and editing. **Marc Schröder:** conceptualization; funding acquisition; supervision; writing – original draft; writing – review



and editing. **Michaela I. Hegglin:** funding acquisition; project administration; supervision; writing – original draft; writing – review and editing. **Luis Gimeno:** conceptualization; funding acquisition; project administration; supervision; writing – original draft; writing – review and editing.

## ACKNOWLEDGEMENTS

This study was funded by ESA (Contract No. 4000123554) via the Water\_Vapour\_cci project of ESA's Climate Change Initiative (CCI). Raquel Nieto, Luis Gimeno, and Jorge Eiras-Barca acknowledge the LAGRIMA Project (RTI2018-095772-B-I00) funded by Ministerio de Ciencia, Innovación y Universidades, Spain, and support from the Xunta de Galicia under the Project ED431C 2017/64-GRC "Programa de Consolidación e Estruturação de Unidades de Investigación Competitivas" (Grupos de Referencia Competitiva). The authors thank the Defense University Center at the Spanish Naval Academy (CUD-ENM) for all the support provided for this research. The authors acknowledge the partial support from the Xunta de Galicia under the Project ED431C 2021/44. The authors acknowledge the funding for open access from the University of Vigo/Consortio Interuniversitario do Sistema Universitario de Galicia.

## CONFLICT OF INTEREST

The authors declare no potential conflict of interest.

## DATA AVAILABILITY STATEMENT

The CDR-2 data are available at <https://www.cmsaf.eu/wui> and the documentation, in particular detailed results from validation, is accessible at <https://climate.esa.int/en/projects/water-vapour/key-documents/> and <https://www.cmsaf.eu/documentation>.

## ORCID

Jorge Eiras-Barca  <https://orcid.org/0000-0003-4401-5944>

## REFERENCES

- Algarra, I., Eiras-Barca, J., Miguez-Macho, G., Nieto, R. and Gimeno, L. (2019a) On the assessment of the moisture transport by the Great Plains low-level jet. *Earth System Dynamics*, 10, 107–119.
- Algarra, I., Eiras-Barca, J., Nieto, R. and Gimeno, L. (2019b) Global climatology of nocturnal low-level jets and associated moisture sources and sinks. *Atmospheric Research*, 229, 39–59.
- Algarra, I., Nieto, R., Ramos, A.M., Eiras-Barca, J., Trigo, R.M. and Gimeno, L. (2020) Significant increase of global anomalous moisture uptake feeding landfalling atmospheric rivers. *Nature Communications*, 11, 1–7.
- Andersson, A., Fennig, K., Klepp, C., Bakan, S., Graßl, H. and Schulz, J. (2010) The Hamburg ocean atmosphere parameters and fluxes from satellite data—HOAPS-3. *Earth System Science Data*, 2, 215–234.
- Blackadar, A.K. (1957) Boundary layer wind maxima and their significance for the growth of nocturnal inversions. *Bulletin of the American Meteorological Society*, 38, 283–290.
- Carbajal Henken, C., Diedrich, H., Preusker, R. and Fischer, J. (2015) MERIS full-resolution total column water vapor: observing horizontal convective rolls. *Geophysical Research Letters*, 42, 10–074.
- Dacre, H.F., Clark, P.A., Martinez-Alvarado, O., Stringer, M.A. and Lavers, D.A. (2015) How do atmospheric rivers form?. *Bulletin of the American Meteorological Society*, 96, 1243–1255.
- Dee, D.P., Uppala, S.M., Simmons, A., Berrisford, P., Poli, P., Kobayashi, S., Andrae, U., Balmaseda, M., Balsamo, G., Bauer, P., Bechtold, P., Beljaars, A.C.M., van de Berg, L., Bidlot, J., Bormann, N., Delsol, C., Dragani, R., Fuentes, M., Geer, A.J., Haimberger, L., Healy, S.B., Hersbach, H., Hólm, E.V., Isaksen, I., Kållberg, P., Köhler, M., Matricardi, M., McNally, A.P., Monge-Sanz, B.M., Morcrette, J.-J., Park, B.-K., Peubey, C., de Rosnay, P., Tavolato, C., Thépaut, J.-N. and Vitart, F. (2011) The ERA-Interim reanalysis: configuration and performance of the data assimilation system. *Quarterly Journal of the Royal Meteorological Society*, 137, 553–597.
- Dettinger, M.D. (2013) Atmospheric rivers as drought busters on the US West Coast. *Journal of Hydrometeorology*, 14, 1721–1732.
- Dettinger, M.D., Ralph, F.M. and Lavers, D.A. (2015) Setting the stage for a global science of atmospheric rivers. *Eos, Earth and Space Science News*, 96.
- Diedrich, H., Preusker, R., Lindstrot, R. and Fischer, J. (2015) Retrieval of daytime total columnar water vapour from MODIS measurements over land surfaces. *Atmospheric Measurement Techniques*, 8, 823–836.
- Dominguez, F., Miguez-Macho, G. and Hu, H. (2016) WRF with water vapor tracers: a study of moisture sources for the North American monsoon. *Journal of Hydrometeorology*, 17, 1915–1927.
- Eiras-Barca, J., Brands, S. and Miguez-Macho, G. (2016) Seasonal variations in North Atlantic atmospheric river activity and associations with anomalous precipitation over the Iberian Atlantic Margin. *Journal of Geophysical Research: Atmospheres*, 121, 931–948.
- Eiras-Barca, J., Dominguez, F., Hu, H., Garaboa-Paz, D. and Miguez-Macho, G. (2017) Evaluation of the moisture sources in two extreme landfalling atmospheric river events using an Eulerian WRF tracers tool. *Earth System Dynamics*, 8, 1247–1261.
- Eiras-Barca, J., Dominguez, F., Yang, Z., Chug, D., Nieto, R., Gimeno, L. and Miguez-Macho, G. (2020) Changes in South American hydroclimate under projected Amazonian deforestation. *Annals of the New York Academy of Sciences*, 1472, 104–122.
- Eiras-Barca, J., Ramos, A.M., Algarra, I., Vázquez, M., Dominguez, F., Miguez-Macho, G., Nieto, R., Gimeno, L., Taboada, J. and Ralph, F.M. (2021) European West Coast atmospheric rivers: a scale to characterize strength and impacts, weather and climate. *Extremes*, 31, 100–305.
- Eiras-Barca, J., Ramos, A.M., Pinto, J.G., Trigo, R.M., Liberato, M.L. and Miguez-Macho, G. (2018) The concurrence of atmospheric rivers and explosive cyclogenesis in the North Atlantic and North Pacific basins. *Earth System Dynamics*, 9, 91–102.
- Espinoza, V., Waliser, D.E., Guan, B., Lavers, D.A. and Ralph, F.M. (2018) Global analysis of climate change projection

- effects on atmospheric rivers. *Geophysical Research Letters*, 45, 4299–4308.
- Fennig, K., Schröder, M., Andersson, A. and Hollmann, R. (2020) A fundamental climate data record of SMMR, SSM/I, and SSMIS brightness temperatures. *Earth System Science Data*, 12, 647–681.
- Fischer, J.R.P., Schröder, M. and Danne, O. (2021). Algorithm Theoretical Baseline Document—Part 1 (ATBD). ESA Water Vapour cci. Version 2.1, January. [Accessed 5th May 2022].
- Gimeno, L., Dominguez, F., Nieto, R., Trigo, R., Drumond, A., Reason, C.J., Taschetto, A.S., Ramos, A.M., Kumar, R. and Marengo, J. (2016) Major mechanisms of atmospheric moisture transport and their role in extreme precipitation events. *Annual Review of Environment and Resources*, 41, 117–141.
- Gimeno, L., Nieto, R., Drumond, A., Castillo, R. and Trigo, R. (2013) Influence of the intensification of the major oceanic moisture sources on continental precipitation. *Geophysical Research Letters*, 40, 1443–1450.
- Gimeno, L., Nieto, R., Vázquez, M. and Lavers, D.A. (2014) Atmospheric rivers: a mini-review. *Frontiers in Earth Science*, 2, 2
- Gimeno, L., Vázquez, M., Eiras-Barca, J., Sorí, R., Stojanovic, M., Algarra, I., Nieto, R., Ramos, A.M., Durán-Quesada, A.M. and Dominguez, F. (2020) Recent progress on the sources of continental precipitation as revealed by moisture transport analysis. *Earth-Science Reviews*, 201, 103070
- Graw, K., Kinzel, J., Schröder, M., Fennig, K. and Andersson, A. (2017). Algorithm Theoretical Baseline Document—HOAPS Version 4.0. EUMETSAT CM SAF ATBD Version 2. [Accessed 15th July 2020].
- He, J., Brogniez, H. and Picon, L. (2022) Evaluation of tropical water vapour from CMIP6 GCMs using the ESA CCI “Water Vapour” climate data records. *Atmospheric Chemistry and Physics Discussions*, preprint, 1–20. <https://acp.copernicus.org/preprints/acp-2021-976/>
- Hersbach, H., Bell, B., Berrisford, P., Hirahara, S., Horányi, A., Muñoz-Sabater, J., Nicolas, J., Peubey, C., Radu, R., Schepers, D., Simmons, A., Soci, C., Abdalla, S., Abellan, X., Balsamo, G., Bechtold, P., Biavati, G., Bidlot, J., Bonavita, M., De Chiara, G., Dahlgren, P., Dee, D., Diamantakis, M., Dragani, R., Flemming, J., Forbes, R., Fuentes, M., Geer, A., Haimberger, L., Healy, S., Hogan, R.J., Hólm, E., Janisková, M., Keeley, S., Laloyaux, P., Lopez, P., Lupu, C., Radnoti, G., de Rosnay, P., Rozum, I., Vamborg, F., Villaume, S. and Thépaut, J.-N. (2020) The ERA5 global reanalysis. *Quarterly Journal of the Royal Meteorological Society*, 146, 1999–2049.
- Holton, J.R. (1967) The diurnal boundary-layer wind oscillation above sloping terrain. *Tellus*, 19, 200–205.
- Insua-Costa, D. and Miguez-Macho, G. (2018) A new moisture tagging capability in the Weather Research and Forecasting model: formulation, validation and application to the 2014 Great Lake-effect snowstorm. *Earth System Dynamics*, 9, 167–185.
- Jiang, X., Lau, N.-C., Held, I.M. and Ploshay, J.J. (2007) Mechanisms of the Great Plains low-level jet as simulated in an AGCM. *Journal of the Atmospheric Sciences*, 64, 532–547.
- Knippertz, P. and Wernli, H. (2010) A Lagrangian climatology of tropical moisture exports to the Northern Hemispheric extratropics. *Journal of Climate*, 23, 987–1003.
- Lavers, D.A., Ralph, F.M., Waliser, D.E., Gershunov, A. and Dettinger, M.D. (2015) Climate change intensification of horizontal water vapor transport in CMIP5. *Geophysical Research Letters*, 42, 5617–5625.
- Lavers, D.A. and Villarini, G. (2013) The nexus between atmospheric rivers and extreme precipitation across Europe. *Geophysical Research Letters*, 40, 3259–3264.
- Lindstrot, R., Preusker, R., Diedrich, H., Doppler, L., Bennartz, R. and Fischer, J. (2012) 1D-Var retrieval of daytime total columnar water vapour from MERIS measurements. *Atmospheric Measurement Techniques*, 5, 631–646.
- Massoud, E., Espinoza, V., Guan, B. and Waliser, D. (2019) Global climate model ensemble approaches for future projections of atmospheric rivers. *Earth's Future*, 7, 1136–1151.
- Miguez-Macho, G. and Fan, Y. (2012) The role of groundwater in the Amazon water cycle: 2. Influence on seasonal soil moisture and evapotranspiration. *Journal of Geophysical Research: Atmospheres*, 117, (D15).
- Myers, L. and Sirois, M.J. (2004) Spearman correlation coefficients, differences between. *Encyclopedia of Statistical Sciences*, 12. <https://doi.org/10.1002/0471667196.ess5050.pub2>
- Nieto, R., Gimeno, L., Drumond, A. and Hernandez, E. (2010) A Lagrangian identification of the main moisture sources and sinks affecting the Mediterranean area. *WSEAS Transactions on Environment and Development*, 6, 365–374.
- Ralph, F.M. and Dettinger, M.D. (2011) Storms, floods, and the science of atmospheric rivers. *Eos, Transactions American Geophysical Union*, 92, 265–266.
- Ralph, F.M., Dettinger, M.D., Rutz, J.J. and Waliser, D.E. (Eds.). (2020) *Atmospheric Rivers* (Vol. 1). Cham, Switzerland: Springer International Publishing.
- Ralph, F.M., Rutz, J.J., Cordeira, J.M., Dettinger, M., Anderson, M., Reynolds, D., Schick, L.J. and Smallcomb, C. (2019) A scale to characterize the strength and impacts of atmospheric rivers. *Bulletin of the American Meteorological Society*, 100, 269–289.
- Ramos, A.M., Nieto, R., Tomé, R., Gimeno, L., Trigo, R.M., Liberato, M.L. and Lavers, D.A. (2016a) Atmospheric rivers moisture sources from a Lagrangian perspective. *Earth System Dynamics*, 7, 371–384.
- Ramos, A.M., Tomé, R., Trigo, R.M., Liberato, M.L. and Pinto, J.G. (2016b) Projected changes in atmospheric rivers affecting Europe in CMIP5 models. *Geophysical Research Letters*, 43, 9315–9323.
- Rife, D.L., Pinto, J.O., Monaghan, A.J., Davis, C.A. and Hannan, J.R. (2010) Global distribution and characteristics of diurnally varying low-level jets. *Journal of Climate*, 23, 5041–5064.
- Saunders, R. (2021) Assimilation of OLCI total column water vapour in the Met Office global numerical weather prediction system. *Meteorological Applications*, 28, e2029
- Schröder, M., Lockhoff, M., Fell, F., Forsythe, J., Trent, T., Bennartz, R., Borbas, E., Bosilovich, M.G., Castelli, E., Hersbach, H., Kachi, M., Kobayashi, S., Kursinski, E.R., Loyola, D., Mears, C., Preusker, R., Rossow, W.B. and Saha, S. (2018) The GEWEX Water Vapor Assessment archive of water vapour products from satellite observations and reanalyses. *Earth System Science Data*, 10, 1093–1117.
- Schröder, M., Lockhoff, M., Shi, L., August, T., Bennartz, R., Brogniez, H., Calbet, X., Fell, F., Forsythe, J., Gambacorta, A., Ho, S.-p., Kursinski, E.R., Reale, A., Trent, T. and Yang, Q. (2019) The GEWEX water vapor assessment: overview and



- introduction to results and recommendations. *Remote Sensing*, 11(3), 251.
- Stohl, A., Forster, C., Frank, A., Seibert, P. and Wotawa, G. (2005) The Lagrangian particle dispersion model FLEXPART version 6.2. *Atmospheric Chemistry and Physics*, 5, 2461–2474.
- SPARC. (2022). SPARC Reanalysis Intercomparison Project (S-RIP) Final Report. In: Masatomo, F., Gloria, L. M., Lesley, J. G. and Jonathon, S. W. (Eds.), SPARC Report No. 10, WCRP-6/2021. <https://doi.org/10.17874/800dee57d13>, available at <https://www.sparc-climate.org/sparc-report-no-10/>.
- Stohl, A. and James, P. (2004) A Lagrangian analysis of the atmospheric branch of the global water cycle. Part I: method description, validation, and demonstration for the August 2002 flooding in central Europe. *Journal of Hydrometeorology*, 5, 656–678.
- Waliser, D. and Guan, B. (2017) Extreme winds and precipitation during landfall of atmospheric rivers. *Nature Geoscience*, 10, 179–183.
- Yu, C., Li, Z. and Blewitt, G. (2021) Global comparisons of ERA5 and the operational HRES tropospheric delay and water vapor products with GPS and MODIS, Earth and Space. *Science*, 8, e2020EA001417.
- Zhu, Y. and Newell, R.E. (1998) A proposed algorithm for moisture fluxes from atmospheric rivers. *Monthly Weather Review*, 126, 725–735.

## SUPPORTING INFORMATION

Additional supporting information can be found online in the Supporting Information section at the end of this article.

**How to cite this article:** Eiras-Barca, J., Algarra, I., Nieto, R., Schröder, M., Hegglin, M.I. & Gimeno, L. (2022) Analysis of the main source regions of moisture transport events with the new ESA CCI/CM-SAF total column water vapour climate data record (v2). *Quarterly Journal of the Royal Meteorological Society*, 1–15. Available from: <https://doi.org/10.1002/qj.4358>